Available online at www.sciencedirect.com
SCIENCE DIRECT®
Polyhedron 22 (2003) 3231–3242
POLYHEDRON
www.elsevier.com/locate/poly

Synthesis, X-ray crystallographic, spectroscopic investigation and cleavage studies of HPNP by simple bispyridyl iron, copper, cobalt, nickel and zinc complexes as artificial nucleases

Thorfinnur Gunnlaugsson [a,*], Mark Nieuwenhuyzen [b,*], Claire Nolan [a]

[a] *Department of Chemistry, Trinity College Dublin, Dublin 2, Ireland*
[b] *School of Chemistry, Queen's University of Belfast, Belfast BT9 5AG, UK*

Received 19 May 2003; accepted 17 July 2003

Abstract

The ligand *N*,*N*-bis[[6-(hydroxymethyl)pyridine-2-yl]methyl]-*p*-tosylamide (**L**) and its Fe(II), Co(II), Ni(II), Cu(I), Cu(II) and Zn(II) complexes were synthesised as potential catalysts for the hydrolysis of phosphate diesters such as 2-hydroxypropyl *p*-nitrophenyl phosphate (HPNP) and mRNA. The ligand and its complexes were characterised by X-ray crystallography, IR, fluorescence and absorption spectroscopy and ESMS. The X-ray structures of **L · Fe(II)**, **[L_1Fe_1]**, **L · Co(II)** **[L_1Co_1]**, **L · Ni(II)** **[L_1Ni_1]** and **L · Zn(II)** **[L_1Zn_1]** showed that there were structurally similar complexes consisting of an octahedral geometry where the metal ion was coordinated to the nitrogens of the two pyridines and to the two hydroxy groups in a square planar arrangement with two CH_3CN molecules capping the two vacant coordination sites. The **L · Cu(II)** however was obtained as a symmetrical dimer **[L_2Cu_2]** from Cu(I). The recognition (complexation) of the in situ complex **L · Cu(I)** (which gave **L · Cu(II)** upon oxidation in air) and **L · Zn(II)** were also investigated by monitoring the changes in the ^{1}H NMR spectrum upon titration with Cu(I) and Zn(II) salts. The **L · Zn(II)** complex was also strongly fluorescent, with a fluorescence enhancement of ca. 200 upon the addition of 1 eq. of $ZnClO_4$. All the compounds hydrolytically cleaved HPNP at pH 7.4 and 37.4 °C, but to different degrees, with **L · Cu(II)** and **L · Zn(II)** being most efficient in promoting transesterification of HPNP.

1. Introduction

Currently there is a great interest in the design and development of small or medium sized organic or organometallic compounds as potential therapeutic agents. Those designed to target nucleic acids site-specifically or to mimic the function of enzymes that participate in nucleic acid strand cleavage are of particular interest, because they can lead to safer and more rational approaches to novel therapeutic agents for cancer, viral diseases and tools for molecular biology [1,2].

Nature has developed both ribozymes and ribonucleases to achieve rapid, site-specific and catalytic cleavage of RNA under physiological conditions. Investigations have shown that the 2′ hydroxy function on the RNA ribose makes hydrolysis or transesterfication much faster than that found for DNA, which lacks this important functionality (Scheme 1) [3]. DNases, RNases, phosphatases and ribozymes all hydrolyse phosphodiester bonds with the direct participation of one or more metal ion centres, such as Mg(II), Zn(II) or Co(II) [3,4]. In many of these, one or more water molecules are directly bound to the metal ion [4]. For enzymes that carry out RNA hydrolysis, the ions participate in the hydrolytic process by either direct (inner sphere) or indirect (outer sphere) activation modes of the 2′ hydroxy function [4,5]. In the former, the metal can stabilize the phosphodiester by: (i) Lewis activation, i.e., by direct metal coordination and (ii) by stabilising the leaving groups upon its expulsion. This is however, thought to be of lesser importance than the role of the metal ion in the nucleophilic activation process of the 2′-hydroxy

* Corresponding authors. Tel.: +353-1-608-3459; fax: +353-1-671-2826 (T. Gunnlaugsson); Tel.: +44-2890-274242; fax: +44-2890-665297 (M. Nieuwenhuyzen).
E-mail addresses: gunnlaut@tcd.ie (T. Gunnlaugsson), woody.m@qub.ac.uk (M. Nieuwenhuyzen).

0277-5387/$ - see front matter © 2003 Elsevier Ltd. All rights reserved.
doi:10.1016/S0277-5387(03)00471-6

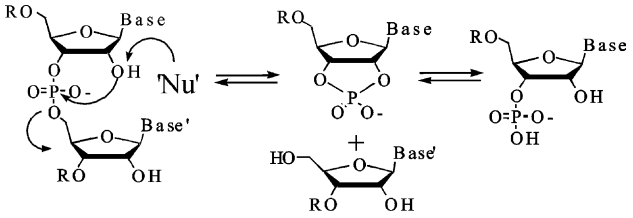

Scheme 1. Hydrolytic cleavage of RNA. *Step 1*: cleavage-transesterification. *Step 2*: hydrolysis of the cyclic phosphodiester. Both the 2′ and 3′ monophosphate (shown) products can be formed. 'Nu' represents a nucleophile or other activating agents such as Lewis acid metal centre or a metal bound water molecule (or hydroxide).

group of the ribose (Scheme 1), which takes place through metal bound water molecules (or hydroxy groups depending on pH) that deprotonate the 2′ hydroxy group which consequently makes it significantly more nucleophilic [3–5]. Because of this, there has been great interest in making synthetic analogues of such biocatalysts and can be used as potential drugs for treating genetically based diseases, which interfere with protein expression at the mRNA level [6–8]. Several mono-, di- and tri-nuclear transition metal compounds have been designed as enzyme mimics and their catalytic ability investigated by employing phosphodiester models and RNA [4,7,8]. A few of these transition metal complexes have been incorporated into oligonucleotide conjugates as potential antisense agents [9,10]. However, many of these metalloenzyme mimics have been made in situ, yielding complexes that are difficult to analyse and often have poor water solubility. Furthermore, free metal ions in solution can give rise to *non-specific* phosphodiester hydrolysis. Additionally, these enzyme mimics often suffer from rather low catalytic turnover. As such, their use for in vivo applications is limited.

We have been perusing the developments of metal-based ribonuclease mimics and have designed several lanthanide complexes from cyclen macrocyclic derivatives as ribonuclease mimics [11], as well as using these lanthanide complexes as luminescent devices [12]. We are also interested in the design of simpler coordination systems based on acyclic ligands that possess a conformationally preorganised geometry, and contain transition metal ions of the type used in nucleases. Our primary goal was to develop simple transition metal complexes that would mimic the active site in ribonucleases, which possess numbers of amino acid residues with acidic, basic, nucleophilic and/or positively charged residues. For instance, in RNase A, a lysine residue activates the phosphoryl group while two histidine residues help in the deprotonation step of nucleophile and the protonation of the leaving group (the 5′ part of the phophodiester, Scheme 1). We chose to use simple pyridine and hydroxy groups to mimic the function of these amino acid residues. With this in mind we set out to make the bispyridyl ligand **L** (*N*,*N*-bis[[6-(hydroxymethyl)pyridine-2-yl]methyl]-*p*--tosylamide), which had previously been made by Miyahara and co-workers [13] as an intermediate in the syntheses of 2,11,20-triaza[3.3.3](2,6)pyridinophane. Simple molecular modelling of **L** suggested that the tosylamide would force the pyridine groups (mimicking the histidine residues) into parallel positions with the two methyl alcohols (mimicking the serine residues) as additional binding sites that had more rotational freedom. In this paper we give full account of the use of these complexes to cleave 2-hydroxypropyl *p*-nitrophenyl phosphate (HPNP), which is a RNA mimic system, Scheme 2, that can be used to evaluate the hydrolytic process under physiological conditions [4,5,7,8,14].

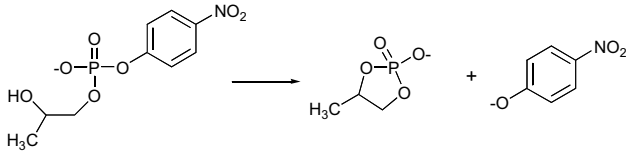

Scheme 2. Hydrolysis of HPNP giving the cyclic phosphate and *p*-nitrophenolate.

2. Results and discussion

2.1. Synthesis of L, and its complexes L · Fe(II), L · Co(II), L · Ni(II), L · Cu(II) and L · Zn(II)

The ligand **L**, Fig. 1, was synthesised using a modified literature procedure [13]. Analysis of this compound was in accordance with that in the literature [13].

The **L · Fe(II)**, **L · Co(II)**, **L · Ni(II)**, **L · Cu(II)** and **L · Zn(II)** complexes were all made by dissolving **L** in CH_3CN and adding one equivalent of the corresponding perchlorate salt $[M(H_2O)_6](ClO_4)_2$ for M = Fe(II), Co(II), Ni(II) and Zn(II). In the case of **L · Cu(II)**, the complex was formed from the Cu(I) salt, under anhydrous conditions in CH_3CN. Oxidation in air afforded **L · Cu(II)** crystals; **L · Cu(I)** was not isolated from this mixture. Unfortunately, we were unable to grow crystals of **L · Cu(II)** obtained by direct synthesis of **L** with Cu(II)-salts. Consequently all hydrolytic measurements were carried out using **L · Cu(II)** formed from oxidising **L · Cu(I)**. For the remaining complexes, **L · Fe(II)**,

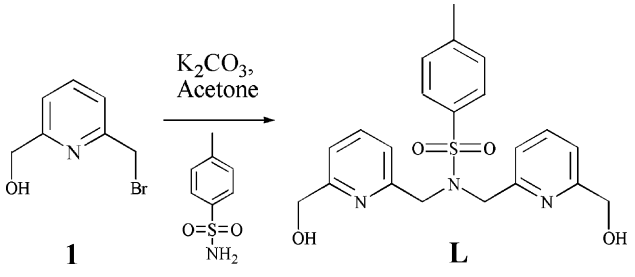

Fig. 1. Synthesis of the ligand (**L**).

L · Co(II), L · Ni(II), **L · Co(II)** and **L · Zn(II)**, crystals were grown by diffusion of diethyl ether into the CH_3CN solutions. All the products were analysed by electrospray MS (ESMS), IR, UV–Vis and (in some cases) fluorescence spectroscopy. The ESMS of all the complexes clearly indicated the formation of the **L · M(II)** species. These isolated crystals of **L · Fe(II)**, **L · Co(II)**, **L · Ni(II)**, **L · Cu(II)** and **L · Zn(II)**, were found to be of sufficient quality for X-ray crystal structure analysis. These crystals were also used when evaluating the hydrolysis of HPNP (see later).

2.2. X-ray crystallographic investigation of L and its complexes

As stated above, we were able to grow crystals of **L**, **L · Fe(II)**, **L · Co(II)**, **L · Ni(II)**, **L · Cu(II)** and **L · Zn(II)** suitable for single crystal X-ray crystallographic determination. Data were collected on a Bruker SMART diffractometer at ca. 153 K [15,16]. Experimental details are listed in Table 1.

The molecular structure of **L** is shown in Fig. 2. The asymmetric unit of the ligand (**L**) contains two independent molecules (A and B) and two water molecules. The conformation of the pyridine moieties is defined by the torsion angle C6–C7–N8–C9 (106° and 91.9°, respectively, for molecules A and B) and gives rise to closest intramolecular ring contacts at 3.2–3.6 Å. This combined with the fact that the angle between the two pyridine moieties is 33.5° and 34.6° for A and B, respectively, indicates that there are no intramolecular π–π stacking interactions within **L**. The sulfonamide nitrogen is pyramidal, being 0.3 Å out of the C7–S20–C9 mean plane, with a torsion angle of 83° and 104° for C7–N8–S20–C21, for molecules A and B, respectively. The methyl hydroxy group conformations are dictated by hydrogen bonding interactions and the torsion angle varies, with three out of four groups (for A and B) being coplanar with respect to the pyridine moieties and the fourth being perpendicular. The molecules are further constrained in the solid-state by extensive O–H···O and O–H···N hydrogen bonds. These interactions lead to the formation of hydrogen bond chains along the *b* axis. The chains are linked into layers via hydrogen bonding of the water molecules with the tosylate moieties extending above and below these layers, creating hydrophilic and hydrophobic regions within the lattice.

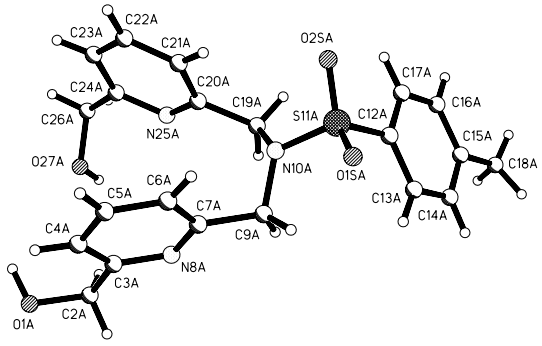

Fig. 2. Molecular structure and numbering scheme for **L**. Atomic displacement parameters at 50%.

The asymmetric unit of **L · Fe(II)** contains one $[Fe(\mathbf{L})(CH_3CN)_2]^{2+}$ cation and two ClO_4^- anions. The ClO_4^- anions are disordered and have been modelled as

Table 1
Data collection and structural refinement details

Empirical formula Reference code	$C_{21}H_{25}N_3O_5S$ **L**	$C_{25}H_{29}Cl_2FeN_5O_{12}S$ **L · Fe(II)**	$C_{27}H_{34}Cl_2CoN_6O_{13}S$ **L · Co(II)**	$C_{25}H_{29}Cl_2NiN_5O_{12}S$ **L · Ni(II)**	$C_{42}H_{44}Cl_2N_6O_{16}S_2Cu_2$ **L · Cu(II)**	$C_{23}H_{30}Cl_2N_4O_{14}SZn$ **L · Zn(II)**
M	431.50	750.34	812.49	753.20	1150.93	754.84
Crystal size (mm)	0.42 × 0.35 × 0.08	0.28 × 0.18 × 0.14	0.46 × 0.14 × 0.08	0.45 × 0.31 × 0.16	0.42 × 0.20 × 0. 04	0.30 × 0.16 × 0.14
Crystal system	monoclinic	monoclinic	monoclinic	triclinic	triclinic	triclinic
Space group (**Z**)	$P2_1/c$ (**8**)	$P2_1/c$ (**4**)	$P2_1/n$ (**4**)	$P\bar{1}$ (**2**)	$P\bar{1}$ (**1**)	$P\bar{1}$ (**2**)
a (Å)	12.347(4)	9.8128(8)	8.8921(7)	9.1323(13)	8.2961(18)	7.4002(5)
b (Å)	14.551(4)	18.1479(14)	18.9983(15)	13.1370(18)	10.329(2)	13.1465(9)
c (Å)	23.593(8)	17.5368(14)	20.5391(16)	13.9096(19)	13.875(3)	15.9724(11)
α (°)	90	90	90	104.946(3)	79.885(4)	83.9660(10)
β (°)	92.868(5)	93.844(2)	93.454(2)	91.743(3)	82.897)4)	86.6680(10)
γ (°)	90	90	90	100.088(3)	78.082(4)	78.4490(10)
U (Å^3)	4234(2)	3116.0(4)	3463.5(5)	1582.3(4)	1140.5(4)	1512.90(18)
D_c (g cm^{-3})	1.354	1.599	1.558	1.581	1.676	1.657
F(000)	1824	1544	1676	776	590	776
μ (Mo K$_\alpha$) (mm^{-1})	0.191	0.792	0.782	0.917	1.221	1.132
ω scans; 2θ range (°)	3–53	3–57	2–58	3–57	3–50	2–58
Transmission (max, min)		0.8972, 0.8086	1.000, 0.900	1.000, 0.752	1.000, 0.743	0.858, 0.728
Unique reflections	8644	7166	7997	6082	3928	6857
*wR*2 (*R*1)	0.1177 (0.0468)	0.1808 (0.0599)	0.1381 (0.0524)	0.1986 (0.0647)	0.2137 (0.0737)	0.1327 (0.0514)

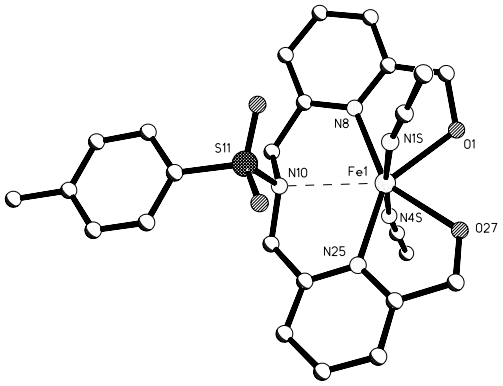

Fig. 3. Diagram illustrating the coordination environment and numbering scheme for **L · Fe(II)**. The dotted line represents the weak coordination by N10.

having two main sites. The cations are hydrogen bonded to the anions via the hydroxyl-oxygen atoms of the Fe(II) complex. The Fe(II) in **L · Fe(II)** is coordinated by one equatorial ligand molecule and two axial acetonitrile molecules Fig. 3. The metal centres are strongly coordinated to the hydroxy moieties and two of the nitrogen atoms of the ligand while the third ligand nitrogen is only weakly coordinated resulting in a seven coordinate metal centre, Table 2. This coordination environment about the metal centre in $[Fe(\mathbf{L})(CH_3CN)_2]^{2+}$ results in the benzyl ring of tosylate moiety being parallel to the two pyridyl rings. Thus, the cations are able to pack together in columns, which are interdigitated forming a 3-D network of $\pi\cdots\pi$ interactions surrounding the perchlorate anions (See CIF File).

The asymmetric unit of **L · Co(II)** contains one $[Co(\mathbf{L})(CH_3CN)_2]^{2+}$ cation, two ClO_4^- anions, two solvent molecules, water and acetonitrile. Unlike the previous structure, the ClO_4^- anions are not disordered. The Co(II) atoms in **L · Co(II)** are coordinated by one equatorial ligand molecule and two axial acetonitrile molecules, Fig. 4. As in **L · Fe(II)** this coordination environment about the metal centre in

Table 2
Selected bond lengths and angles

L · Fe(II)				**L · Ni(II)**			
Fe(1)–N(4S)	2.170(4)	N(4S)–Fe(1)–O(27)	90.54(14)	Ni(1)–O(1)	2.036(3)	O(1)–Ni(1)–O(27)	91.44(13)
Fe(1)–O(27)	2.173(3)	N(4S)–Fe(1)–N(25)	86.94(13)	Ni(1)–O(27)	2.051(3)	O(1)–Ni(1)–N(1S)	89.93(14)
Fe(1)–N(25)	2.178(4)	O(27)–Fe(1)–N(25)	71.94(15)	Ni(1)–N(1S)	2.073(4)	O(27)–Ni(1)–N(1S)	84.91(14)
Fe(1)–N(8)	2.180(4)	N(4S)–Fe(1)–N(8)	90.71(13)	Ni(1)–N(4S)	2.078(4)	O(1)–Ni(1)–N(4S)	87.15(14)
Fe(1)–N(1S)	2.186(4)	O(27)–Fe(1)–N(8)	146.12(15)	Ni(1)–N(25)	2.094(4)	O(27)–Ni(1)–N(4S)	92.31(14)
Fe(1)–O(1)	2.216(3)	N(25)–Fe(1)–N(8)	141.93(14)	Ni(1)–N(8)	2.113(3)	N(1S)–Ni(1)–N(4S)	175.92(15)
		N(4S)–Fe(1)–N(1S)	173.89(14)			O(1)–Ni(1)–N(25)	170.53(13)
		O(27)–Fe(1)–N(1S)	86.34(14)			O(27)–Ni(1)–N(25)	79.85(13)
		N(25)–Fe(1)–N(1S)	97.06(13)			N(1S)–Ni(1)–N(25)	92.96(14)
		N(8)–Fe(1)–N(1S)	88.97(14)			N(4S)–Ni(1)–N(25)	89.48(14)
		N(4S)–Fe(1)–O(1)	90.69(13)			O(1)–Ni(1)–N(8)	76.91(13)
		O(27)–Fe(1)–O(1)	73.84(15)			O(27)–Ni(1)–N(8)	166.95(13)
		N(25)–Fe(1)–O(1)	145.66(15)			N(1S)–Ni(1)–N(8)	89.17(14)
		N(8)–Fe(1)–O(1)	72.29(14)			N(4S)–Ni(1)–N(8)	92.94(14)
		N(1S)–Fe(1)–O(1)	83.40(13)			N(25)–Ni(1)–N(8)	112.12(14)
L · Co(II)				**L · Cu(II)**			
Co(1)–N(4S)	2.103(3)	N(4S)–Co(1)–N(1S)	174.56(12)	Cu(1)–O(1)′	1.908(5)	O(1)–Cu(1)–O(1)′	78.4(2)
Co(1)–N(1S)	2.131(3)	N(4S)–Co(1)–N(25)	94.22(11)	Cu(1)–O(1)	1.924(5)	O(1)–Cu(1)–N(8)′	157.6(2)
Co(1)–N(25)	2.174(3)	N(1S)–Co(1)–N(25)	88.11(11)	Cu(1)–N(8)	2.001(6)	O(1)–Cu(1)–N(8)	80.2(2)
Co(1)–N(8)	2.175(3)	N(4S)–Co(1)–N(8)	92.60(11)	Cu(1)–N(25)	2.026(6)	O(1)–Cu(1)–N(25)′	95.6(2)
Co(1)–O(27)	2.194(3)	N(1S)–Co(1)–N(8)	88.53(11)	Cu(1)–O(27)	2.428(6)	O(1)–Cu(1)–N(25)	162.4(3)
Co(1)–O(1)	2.214(3)	N(25)–Co(1)–N(8)	142.33(12)	Cu(1)–Cu(1)′	2.970(2)	N(8)–Cu(1)–N(25)	106.8(3)
		N(4S)–Co(1)–O(27)	86.60(11)			O(1)–Cu(1)–O(27)′	92.7(2)
		N(1S)–Co(1)–O(27)	89.40(11)			O(1)–Cu(1)–O(27)	87.7(2)
		N(25)–Co(1)–O(27)	72.73(11)			N(8)–Cu(1)–O(27)	93.1(2)
		N(8)–Co(1)–O(27)	144.73(11)			N(25)–Cu(1)–O(27)	76.0(2)
		N(4S)–Co(1)–O(1)	83.67(11)				
		N(1S)–Co(1)–O(1)	91.57(11)	**L · Zn(II)**			
		N(25)–Co(1)–O(1)	144.45(11)	Zn(1)–O(1W)	2.002(2)	O(1W)–Zn(1)–N(8)	138.22(10)
		N(8)–Co(1)–O(1)	73.14(10)	Zn(1)–N(8)	2.040(3)	O(1W)–Zn(1)–N(25)	97.27(10)
		O(27)–Co(1)–O(1)	71.73(10)	Zn(1)–N(25)	2.092(3)	N(8)–Zn(1)–N(25)	110.76(10)
				Zn(1)–O(27)	2.109(2)	O(1W)–Zn(1)–O(27)	100.44(10)
				Zn(1)–O(1)	2.134(2)	N(8)–Zn(1)–O(27)	115.72(11)
						N(25)–Zn(1)–O(27)	75.89(10)
						O(1W)–Zn(1)–O(1)	90.08(9)
						N(8)–Zn(1)–O(1)	76.10(10)
						N(25)–Zn(1)–O(1)	157.09(11)
						O(27)–Zn(1)–O(1)	81.46(10)

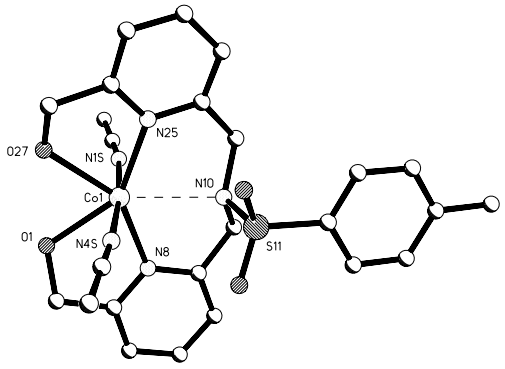

Fig. 4. Diagram illustrating the coordination environment and numbering scheme for **L · Co(II)**. The dotted line represents the weak coordination by N10.

$[Co(\mathbf{L})(CH_3CN)_2]^{2+}$ results in the benzyl ring of the tosylate moiety being approximately parallel to the two pyridyl rings. Again, the cations are able to pack together in columns that are interdigitated forming a 3-D network of $\pi\cdots\pi$ interactions surrounding the perchlorate anions. Furthermore, as in **L · Fe(II)** the metal centres are strongly coordinated to the two hydroxy moieties and two of the nitrogen atoms of the ligand while the third ligand nitrogen is only weakly coordinated resulting in a seven coordinate metal centre, Figs. 3 and 4. The orientation of the nitrogen atoms (N10) in both **L · Fe(II)** and **L · Co(II)** is facilitated by the fact that the $d_{x^2-y^2}$ orbital on each metal centre is vacant. It should be noted that the weakly bound nitrogen (N10) in both complexes is pyramidal with the lone pair 'directed' towards the metal centre.

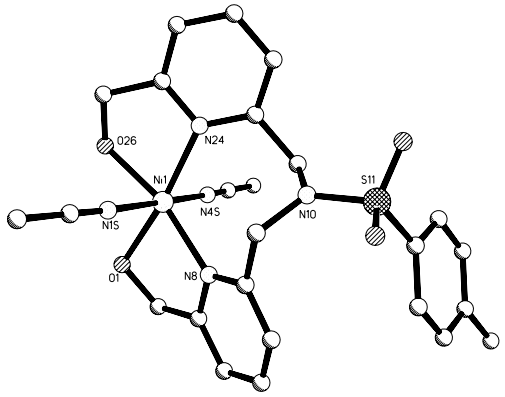

Fig. 5. Coordination environment and labelling scheme of **L · Ni(II)**.

The asymmetric unit of **L · Ni(II)** contains one $[Ni(\mathbf{L})(CH_3CN)_2]^{2+}$ cation and two ClO_4^- anions. The cations are hydrogen bonded to the anions via the hydroxyl oxygen atoms of the Ni(II) complex. The Ni(II) atoms in **L · Ni(II)** are coordinated by one equatorial ligand molecule and two axial acetonitrile molecules, resulting in a distorted octahedral metal centre, Fig. 5. As seen before, the metal centres are strongly coordinated to the two hydroxy moieties and two of the nitrogen atoms of the ligand. The ligand adopts a conformation that is significantly different from that in **L · Fe(II)** and **L · Co(II)**.

It was noticeable that the lone pair on N10 is no longer directed towards the metal centre. Furthermore, the benzyl ring of the tosylate is no longer parallel to the two pyridyl rings of the ligand, in fact they are almost orthogonal. This alters the packing of the cations significantly and the cations are now associated into layers linked via two types of $\pi\cdots\pi$ interactions: (1) inter-tosylate along the *a* axis and (2) inter-pyridyl (N24–N24) along the *b* axis. The layers pack together in such a way that the methyl groups of the acetonitrile molecules are directed towards the other pyridyl group of **L**.

In **L · Cu(II)** the coordination of the Cu(II) centres is best described as square-based pyramidal, Table 2. Unusually **L · Cu(II)** exists as a dimer with one of the hydroxyl groups being deprotonated and acting as the bridging moiety, Fig. 6. The 'vacant' coordination sites are occupied by the sulfonamide functionalities with the lone pair associated with N10 directed towards the metal centre with the Cu···Cu contact at 2.970 Å. Furthermore, unlike the complexes discussed above the Cu(II) centres are no longer equatorially coordinated by **L** and they do not contain solvent molecules.

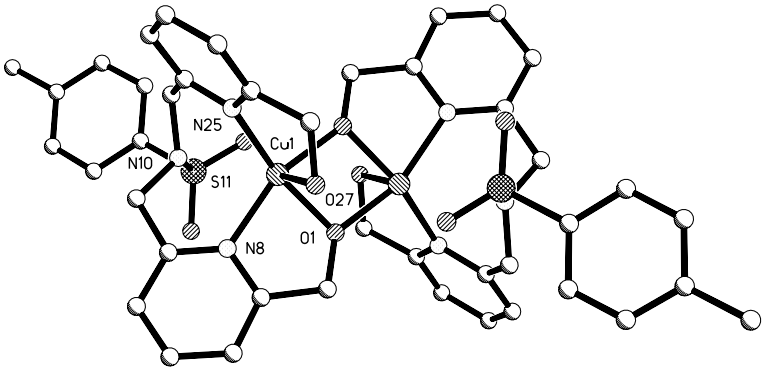

Fig. 6. Coordination environment of **L · Cu(II)**. The copper ions are related by an inversion centre.

In **L · Zn(II)** the Zn(II) centres are not equatorially coordinated by **L**, rather the coordination of the Zn(II) centres is best described as distorted trigonal bipyramidal with the apical atoms of the trigonal bipyramid being N10 and O1W, Table 2. The coordination of the Zn(II) centres is illustrated in Fig. 7. It is perhaps significant that the conformations of **L** in **L · Cu(II)** and **L · Zn(II)** are very similar. This is seen from a comparison of the dihedral angle of the backbone at −142.5° and −132.9° and the angle between the mean planes of the pyridyl groups of 101.5° and 81.5° for **L · Zn(II)** and **L · Cu(II)**, respectively. As in **L · Fe(II)**, the nitrogen N10 is able to direct the associated lone pairs towards the metal centre (Zn–N10, 2.619 Å).

A comparison of the torsion angle of C7–C9–N10–C19 backbone for the coordination complexes **L · M(II)** shows that **L** in four of the five complexes has a similar conformation. The torsion angles are angles of 66°, −153°, −150°, −133° and −143° for M = Ni (II), Fe(II), Co(II), Cu(II) and Zn(II), respectively. It is also instructive to examine the relative orientation of the pyridyl and benzyl rings to one another in these complexes. In **L · Fe(II)**, **L · Co(II)** and **L · Ni(II)** the pyridyl rings are essentially coplanar with the angle between them being 15°, 8° and 37°, respectively. In contrast, the angle of these rings to the benzyl moiety is 12° to C3–C4–C5–C6–C7–N8 and 3.4° to C20–C21–C22–C23–C24–N25 for **L · Fe(II)**, 1.7° to C3–C4–C5–C6–C7–N8 and 9.3° to C20–C21–C22–C23–C24–N25 for **L · Co(II)** and 108° to C3–C4–C5–C6–C7–N8 and 73° to C20–C21–C22–C23–C24–N25 for **L · Ni(II)**. While the metal centres of all three of these complexes have a distorted octahedral coordination sphere, the distortion of the Fe(II) and Co(II) complexes are more pronounced with a maximum deviation of 17–18° from 90° for the O1–N8 and O27–N25 bite angles for **L · Fe(II)** and **L · Co(II)** compared to 13° and 10° for the O1–N8 and O27–N25 bite angles in **L · Ni(II)**, Table 2. The smaller bite angles in **L · Fe(II)** and **L · Co(II)** may be due to the increased constraint placed upon the ligand because of the weaker M–N10 interaction which pulls the ligand more tightly on to the metal centre.

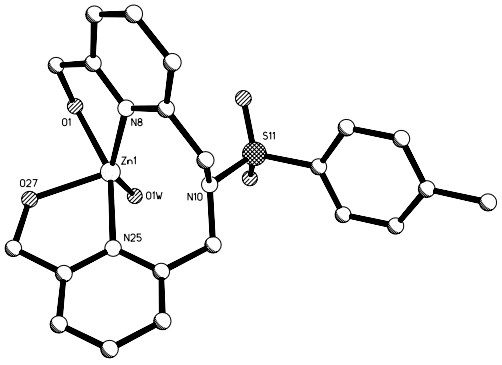

Fig. 7. The coordination environment of **L · Zn(II)** illustrating the distorted trigonal bipyramidal coordination of the metal.

3. Ligand investigations

3.1. ^{1}H NMR spectroscopic investigation of **L · Cu(I)** *and* **L · Zn(II)**

Although we were unable to isolate the **L · Cu(I)** complex directly, we were able to monitor the formation of this species by monitoring the changes in the ^{1}H NMR spectra of **L**, in CD_3CN, upon addition of a Cu(I) salt. Such ^{1}H NMR titrations were also carried out for Zn(II) in CD_3CN and in DMSO-d_6. It was hoped that the nature of the interactions of these ions with the free ligand could be elucidated by these experiments.

Fig. 8 shows the changes in the ^{1}H NMR spectrum of **L** upon addition of Cu(I) perchlorate salt in CD_3CN. The free ligand showed two resonances at 4.55 and 4.49 ppm (numbered as *a* and *b*, respectively, in Fig. 8), indicating that the compound had C_2 symmetry. These

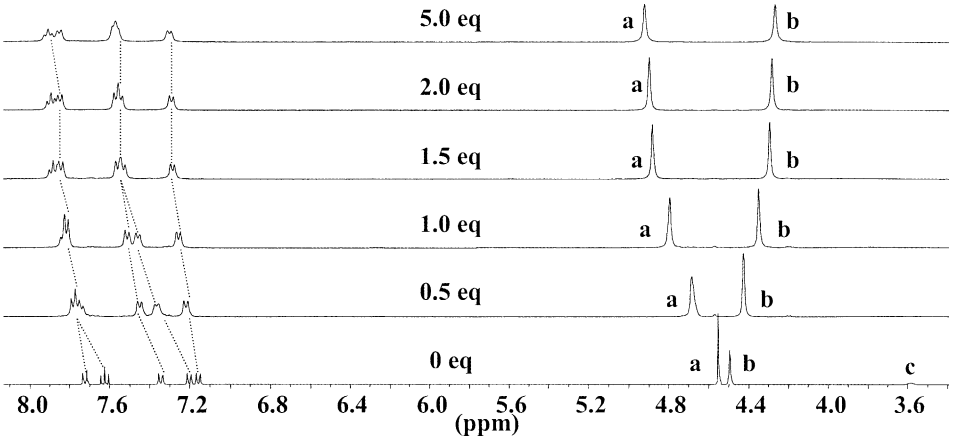

Fig. 8. Changes in the ^{1}H NMR spectrum (400 MHz, CD_3CN) of **L** upon addition of copper perchlorate.

signals were assigned to the two CH_2 moieties in **L**, where *b* (Fig. 8) was assigned to the CH_2 adjacent to the hydroxide group of the two arms. In dry CD_3CN or in DMSO-d_6 this signal was observed as doublet coupled to the O–H, which appears at δ 3.58 in Fig. 8 (labelled as *c*). Subsequently, resonance *a* was assigned to the CH_2 on the other side of the sulfonamide. Upon addition of 0.5 and 1 equivalent of Cu(I) perchlorate the *a* and *b* resonance shifted substantially: *a* was shifted upfield to 4.79 ppm and *b* downfield to 4.35 ppm after one equivalent of Cu(I), indicating the formation of a new Cu(I)–**L** complex. The disappearance of the hydroxy signal at 3.58 (*c*) suggested the two hydroxyl groups were participating directly in metal ion coordination. Further changes were also seen in the aromatic region. Of these, the two doublets and triplet signals assigned to the protons of the pyridine moieties, and resonating at 7.20, 7.16 and 7.62 ppm, respectively, were most affected due to direct coordination of the two nitrogen moieties to the Cu(I) centre. Upon further addition of Cu(I) the *a* and *b* resonance became even more shifted and after the addition of 2 equivalents, they had shifted to 4.90 and 4.28 ppm, respectively. The aromatic region also changed, showing three sets of signals: a doublet at 7.30, a triplet at 7.56 and a multiplet at 7.87 ppm. No further changes were observed upon addition of further equivalents of Cu(I).

For the titration of **L** with Zn(II) perchlorate salt, the ^{1}H NMR spectral changes were similar to those seen above. The hydroxide signal, *c*, was found to be substantially broadened, and after the addition of 5 equivalents of Zn(II), the two methyl signals *a* and *b* had substantially shifted in a similar fashion to the Cu(I) titration above. Upon addition of a further 3 equivalents of Zn(II) there was a significant sharpening of all the resonances, with the *a* and *b* appearing as a clear singlets at δ 5.03 and 4.39 ppm, respectively. After 12 equivalents of Zn(II), a triplet, two doublets and multiplet appeared at 8.14, 7.82, 7.64 and 7.52 ppm, respectively, indicating the formation of the new species **L · Zn(II)**. We did not determine the binding constant for the complexation by this method. Instead this was achieved by observing the changes in the absorption and the fluorescence spectra of **L** upon titration of the ligand using the above metal ion salts, see next section.

3.2. Ground and excited state investigation of **L** and its complexes

The ground and excited state behaviour of **L** was investigated in both CH_3CN and H_2O. The absorption spectra of **L** in CH_3CN consisted of two absorption bands at 231 and 267 nm and a shoulder at 274 nm, Fig. 9. Upon titration of **L** (ca. 1 μM) with zinc perchlorate ($0 \rightarrow 0.32$ mM) the intensity of the 267 nm band (which was assigned to the pyridine components of **L**) was reduced in intensity and slightly blue shifted to 265 nm with an isosbestic point at 256 nm. The 231 nm band was also affected by the addition of Zn(II) with the absorption being slightly red shifted. The addition of Cu(I), Cu(II) and Ni(II) salts to the solution of **L** also gave rise to spectral changes; for Cu(II) the absorption at 274 nm increased slightly whereas for Ni(II) the intensity of this band was reduced, similar to that seen for Zn(II). From these changes the binding constant $\log\beta$ was determined [17]. [1] Plotting the absorption changes at 264 nm as a function of pM (where $pM = -\log[M]$, $M = Zn(II)$), gave a sigmoidal curve indicating 1:1 binding and simple equilibrium. From these changes the $\log\beta$ was determined to be 4.4 (±0.1). For Cu(II) and Ni(II) $\log\beta$ was found to be 4.7 (±0.1) and 4.5 (±0.1), respectively, indicating that **L** showed no selective binding for one of these metal ions over the others.

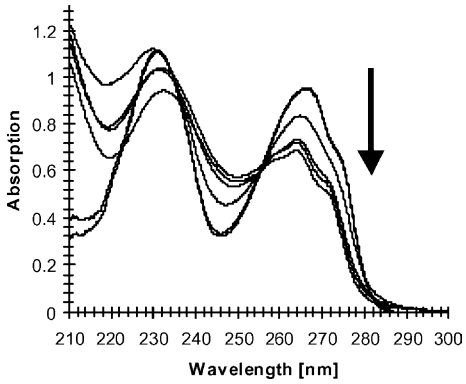

Fig. 9. Absorption spectra of **L** in the absence and the presence of Zn(II); in decreasing order of Zn(II) concentration; [Zn(II)] = $0 \rightarrow 0.32$ mM.

The changes in the fluorescence spectra were more striking. Zn(II) is known to give rise to strong fluorescence in the presence of pyridine and pyridine-like ligands such as 1,10-phenanthroline and bipyridine due to the presence of emissive MLCT excited states [18]. In the absence of Zn(II), the fluorescence emission spectrum of **L** in CH_3CN consisted of a major emission band centred at 295 nm and a shoulder at 345 nm when excited at 267 nm. Upon addition of Zn(II) the MLCT-based fluorescence emission was gradually *switched on* with a fluorescence enhancement of ca. 23, when measured at 300 nm (Fig. 10). The fluorescence emission was also slightly red shifted upon addition of Zn(II), from 293 to 300 nm. Plotting the emission changes at 300 nm as a function of

[1] The binding constant was determined from the changes in the absorption and the fluorescence emission spectra using the equation: $\log[\text{guest}] = \log[(I_F I_{F\min})/(I_{F\max} - I_F)] - \log\beta$ for the changes in the fluorescence spectra and the equivalent equation was used for determining the changes in the absorption spectra: $\log[\text{guest}] = \log[(A - A_{\min})/(A_{\max} - A)] - \log\beta$.

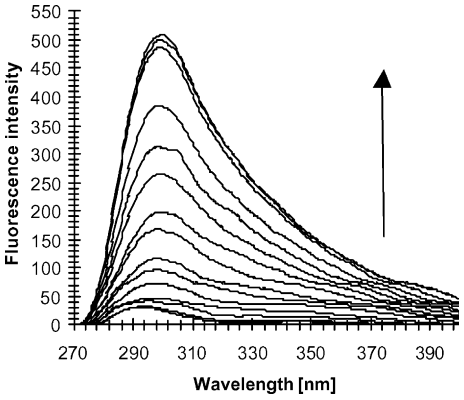

Fig. 10. Changes in fluorescence emission spectra of **L** upon addition of Zn(II) when excited at 275 nm.

added Zn(II) indicated a 1:1 binding, Fig. 11 with a $\log \beta$ of 4.4 (± 0.1). In contrast, the addition of Cu(II) to **L** leads to fluorescence quenching where the emission at 300 nm was fully quenched after the addition of 0.16 mM of Cu(II). This is as expected as Cu(II) is able to participate in photoinduced electron transfer mechanism with the excited state of the ligand, which subsequently is quenched [17]. No major changes were seen in the fluorescence emission spectra of **L** upon addition of Ni(II) perchlorate salt. These measurements were repeated in water at pH 7.0 using 0.1 mM Tris buffer and in the presence of tetramethylammonium chloride to maintain constant ionic strength. Unlike the results seen in CH_3CN, the addition of Ni(II) yielded some changes in the fluorescence spectra at high concentration, but no changes were seen in the absorption spectrum. Addition of Zn(II) perchlorate or chloride salt showed similar behaviour to that seen in CH_3CN, with the exception that the enhancement factors were smaller, with a $\log \beta$ of 2.4 (± 0.1). Determination of Cu(II) was not possible due to solubility problems. These results suggest that Zn(II) can be detected selectively over Cu(II) and Ni(II) in either solvents. **L** is thus a fluorescent chemosensor for Zn(II).

3.3. Cleavage of the phophodiester of 2-hydroxypropyl p-nitrophenyl phophate by **L · Fe(II)**, **L · Cu(II)**, **L · Ni(II)**, **L · Co(II)** and **L · Zn(II)**

For all the measurements carried out on HPNP herein crystalline material of **L · Fe(II)**, **L · Cu(II)**, **L · Ni(II)**, **L · Co(II)** and **L · Zn(II)** was used, i.e., none of the complexes were made and tested in situ. The model compound HPNP used absorbs strongly at 300 nm (Fig. 12a). Upon hydrolytically cleaving the phosphodiester, using the various complexes described above, two new products, *p*-nitrophenolate that absorbs at 400 nm, and a cyclic phosphate are formed in accordance with Scheme 2.

The changes in the intensity of the 400 nm absorption can be used to evaluate the kinetics of the hydrolytic process (Scheme 1). The cleavage of HPNP was carried out at pH 7.4 in the presence of 50 mM of Hepes buffer and at 37.4 °C. The changes in 400 nm absorption band were monitored by using Agilent photodiode array UV–Vis spectrometer fitted to a circulating temperature controlled water bath, and water driven mechanical stirring. Fig. 12 shows typical changes observed over 16 h in the absorption spectra upon cleavage of HPNP for **L · Zn(II)**. On all occasions an equimolar amount of the complex and HPNP was used. Unfortunately the complexes of **L** absorb in the same region as HPNP (the combination of these two spectra is shown as B in Fig. 12. However, the changes at longer wavelength (400 nm) correspond solely to the formation of the *p*-nitrophenolate (Scheme 2). These absorption changes were plotted as a function of time to give 'typical' kinetic curves, which are best described as pseudo first order. The rate constant k was determined by fitting these observed data to first order rate kinetics using *Biochemical*

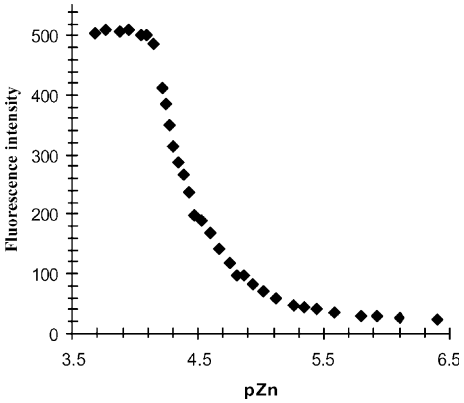

Fig. 11. The pZn ($-\log[Zn(II)]$) as a function of fluorescence intensity. The graph shows the emission being switched on over two pZn units, and indication of 1:1 binding and simple equilibrium.

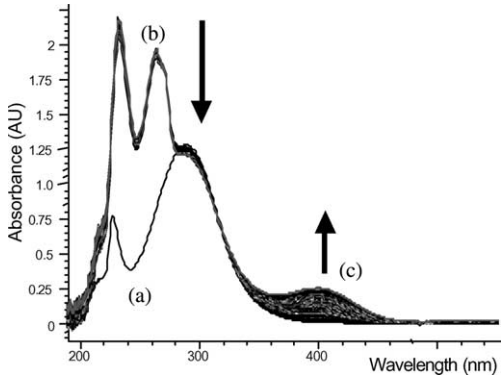

Fig. 12. The changes in the UV–Vis spectra of HPNP upon hydrolysis using **L · Ni(II)**. Graph a is HPNP; b is the combined spectra of **L · Ni(II)** and HPNP; and c shows the growing of the band at 400 nm, which is assigned to the formation of *p*-nitrophenolate.

Analysis Software for Agilent ChemStation. The data were also fitted using zero and initial rate orders. We estimated that the errors in these measurements are within ±15%.

The obtained rate enhancement factors k_{obs}, were obtained from the ratio of the 'catalysed' versus the 'uncatalysed' reaction using $k_{ucat} = 0.00012$ h^{-1} [14]. It became obvious from these measurements that **L · Cu(II)** was the most active of the complexes tested with rate of hydrolysis $k = 0.1206$ h^{-1}. This gives a half-lifetime of 5.7 h, and $k_{obs} = 1005$. These are obtained as averages over 2–3 runs. The remaining complexes showed a rate of hydrolysis of HPNP, with **L · Zn(II)** giving $k = 0.101$ h^{-1}, with a half-lifetime of 6.86 h, and $k_{obs} = 842$. For **L · Co(II)**and **L · Ni(II)**the half-lifetimes were measured to be ca. 13 and 21 h, respectively, with k_{obs} as 444 and 275, respectively. Unfortunately, the **L · Fe(II)** complex was found to be almost completely in comparison to those above.

We propose that the reasons for the relatively fast hydrolysis observed when **L · Cu(II)** was used may be twofold. First, the complex has two metal ions present that can contribute to increased Lewis acid activation versus the mono-metallic complexes. Such dinuclear complexes have previously been shown to give rise to faster hydrolysis than mono-nuclear complexes, where both of the metal centres synergistically participate in the activation and hydrolysis of the phosphodiester [4]. However, even though the X-ray crystal structure indicated that **L · Cu(II)** is a symmetrical dimer **[L_2Cu_2]** then in solution it is possible that it exists as a monomeric complex **[LCu]** and this in fact might give rise to faster hydrolysis as the ion can then bind more strongly to the phosphate. Unfortunately, we were unable to obtain conclusive evidence as to the actual stoichiometry of this complex in solution. Second, it is possible that the leaving group (the phosphate) would be more stabilised by the **L · Cu(II)** complex than the other complexes, though again we were not able to confirm this experimentally.

The **L · Zn(II)** complex which shows the second fastest hydrolysis of HPNP, has in the solid-state structure, as shown in Fig. 7 a metal bound water molecule. Such water molecules have lower pK_a values than non-metal bound water molecules [18]. Hence, these can participate in the nucleophilic activation of the 2′ hydroxy group on the RNA ribose by facilitating deprotonation of the hydroxy group. The same is possible for the activation of the hydroxy group in HPNP. This may possibly be the reason for the much higher rate of hydrolysis than that seen for **L · Co(II)** and **L · Ni(II)**. Even with the bound water molecule, **L · Zn(II)** has a smaller rate constant for the hydrolysis of HPNP than **L · Cu(II)**. Again, if the kinetically activated form of **L · Cu(II)** were the mono-nuclear Cu(II) complex it would possibly also contain such metal bound water molecules. We are currently perusing these lines of investigation.

4. Conclusion

We set out to develop simple ligands possessing functional groups resembling those found in the active sites of many ribonucleases, i.e., **L**. From this we have synthesised several transition metal complexes of **L**. We were able to grow crystals of all the complexes analysed and the ligand **L** suitable for X-ray crystallographic analysis. For all the complexes investigated, the metal ions were complexed by coordinating to the two nitrogen moieties of the pyridyl unit and the two hydroxy groups of the side arms. For **L · Co(II)** and **L · Fe(II)** the ions were also weakly coordinating to the nitrogen moiety of the sulfonamide. The formation of the Cu(I) (which upon oxidation gave the Cu(II) complex) and Zn(II) complexes of **L** was monitored in situ by observing the changes in the ^{1}H NMR spectrum of **L** and in the absorption and the fluorescence spectra of **L** upon titration of these cations.

The ability of these complexes to cleave the RNA model compound HPNP has been investigated. Unfortunately, the rate constants for the hydrolysis (k) were somewhat smaller than we had hoped for in comparison to several cylen-based lanthanide complexes [11]. **L** had been chosen for its relatively open structure so that vacant coordination sites would be occupied by water molecule or other solvent molecules. This would be expected to give rise to faster hydrolysis due to increased nucleophilic activation of the hydroxy group of HPNP. However, only **L · Zn(II)** and **L · Cu(II)** were able to fulfill this criterion successfully. We are currently modifying **L** with the aim of improving the ability of its complexes to further promote cleavage of HPNP through phosphodiester hydrolysis.

5. Experimental

Reagents (obtained from Aldrich) and solvents were purified using standard techniques. Solvents were dried over the appropriate drying agent before use using standard procedures. The ^{1}H (400.13 MHz) and ^{13}C (100.6 MHz) NMR spectra were recorded on a Bruker DPX 400. Mass spectra and accurate masses were recorded on a Micromass LCT instrument with methanol as a carrier solvent unless otherwise stated. UV–Vis absorption spectra were recorded at 20–25 °C using UNI-CAM (UV2) spectrometer and on a Shimadzu UV-2401PC. Kinetic measurements were recorded on Agilent UV–Vis photodiode array spectrometer fitted to circulating temperature controlled water bath and water driven mechanical stirring. Fluorescence emission spectra were recorded on Perkin–Elmer LS50B, and are uncorrected. Throughout the titration experiments, the ligand and complex solution were in the concentration range of $5–7 \times 10^{-5}$ M. Aliquots of 3 cm^{-3} were taken

for absorption and luminescence measurements in standard quartz cuvettes with a 1 cm path length. The appropriate amount of the Zn(II), Cu(I), Cu(II) or Ni(II) (from freshly made stock solutions) was added using micropipettes. Determination of $\log\beta$ values was according to published procedures [17]. Melting points were recorded on a Gallencamp melting point apparatus and are uncorrected. IR spectra were measured using a Perkin–Elmer FT-IR Paragon 100 spectrometer using KBr plates. TLCs were carried out using Merck–Keiselgel 60 F_{254} or neutral alumina and were visualized by using a UV lamp and I_2. Flash column chromatography was carried out using Merck–Keiselgel silica 70–230 mesh. All solvents for chromatographic use were freshly distilled before use.

Crystal data were collected using a Bruker SMART diffractometer with graphite monochromated Mo K_α radiation at ca. 150 K in a dinitrogen stream. Crystal stability were checked and there were no significant variations ($< \pm 1\%$). $\tilde{\omega}$phi scans were employed for data collection and Lorentz and polarisation corrections were applied. The structures were solved by direct methods and the non-hydrogen atoms were refined with anisotropic thermal parameters. Except for **L**, where hydrogen atoms were located and refined, hydrogen-atom positions were added at idealised positions a riding model with fixed thermal parameters ($U_{ij} = 1.2U_{eq}$ for the atom to which they are bonded (1.5 for Me)), was used for subsequent refinements. The function minimised was $\sum[\omega(|F_o|^2 - |F_c|^2)]$ with reflection weights $\omega^{-1} = [\sigma^2|F_o|^2 + (g_1P)^2 + (g_2P)]$, where $P = [\max|F_o|^2 + 2|F_c|^2]/3$. The SAINT-NT [15] and SHELXTL [16] program packages were used for data reduction and structure solution and refinement.

5.1. Synthesis of **L** by modified literature procedure [13]

2-Bromomethyl-6-hydroxymethylpyridine (**1**), was made from 2,6-bis(hydroxymethyl)pyridine by refluxing in 48% HBr for 22 h. After neutralisation with the addition of 40% NaOH, the resulting solution was allowed to cool to room temperature and then stored in the refrigerator overnight. This gave off-white crystals that were isolated and dried giving the desired product and also bis(bromomethyl)pyridine as a 60:40 mixture. These were separated using flash silica column chromatography. Elution, using 100% CH_2Cl_2 gave the bisbromo product, but gradual addition of $0 \rightarrow 5\%$ MeOH gave **1**, which was further reacted with *p*-toluenesulfonamide in the presence of K_2CO_3 in refluxing acetone under anhydrous conditions for 4 days giving **L** as colourless crystals in 82% yield after filtration and removal of the solvent under reduced pressure. Analysis of this material were in accordance to the literature.

5.2. General procedure for complex synthesis

To a solution of **L** (0.05 g, 1.21×10^{-4} mol) in acetonitrile (10 ml) was added equimolar equivalents of the appropriate perchlorate metal salt, and these were stirred for several hours at room temperature. The solutions were then allowed to stand at room temperature for approximately 2 days under a diethyl ether atmosphere, whereupon crystals were observed. These were collected by filtration, washed with cold acetonitrile and dried under vacuum in the presence of P_2O_5.

L · Cu(II): procedure as described above, using $[Cu(MeCN)_4]ClO_4$ (1.21×10^{-4} mol). This sample oxidises in air over time to give the **L · Cu(II)** species. The resulting product was collected as green crystals (85% yield), mp 221.6 °C. Calculated for $C_{42}H_{44}Cl_2N_6O_{16}S_2Cu_2 \cdot H_2O$: C, 43.15; H, 3.97; N, 7.19. Found: C; 43.04; H, 3.74; N, 6.73%; ESMS: m/z 477.0781 (M + 1). λ_{max} (nm) (CH_3CN) 225 (ε ($dm^3\ mol^{-1}\ cm^{-1}$) 8023.7) 265 (6247). ν (cm^{-1}) (KBr discs) 3486m (O–H), 2924w (S–N), 1609m, 1585, 1435m (C=C) (C=N), 1353m, 1164m (S=O), 1091s (ClO_4).

L · Zn(II): procedure as described above, using $[Zn(H_2O)_6]ClO_4$ (1.21×10^{-4} mol). Complex was collected as white crystals (75% yield); mp. 191.5 °C. Calculated for $C_{23}H_{30}Cl_2N_4O_{14}SZn \cdot H_2O$: C, 35.74; H, 4.17; N, 7.25. Found: C; 35.83; H, 3.66; N, 7.10%; ESMS: m/z 557 (M^+). λ_{max} (nm) (CH_3CN) 223 (ε ($dm^3\ mol^{-1}\ cm^{-1}$) 6421.6) 266 (2868). ν (cm^{-1}) (KBr discs) 3412b (O–H) (S–N), 1610m, 1588, 1439m (C=C) (C=N), 1354m (S=O), 1089s.

L · Ni(II): procedure as described above, using $[Ni(H_2O)_6]ClO_4$) (1.21×10^{-4} mol). Complex was collected as blue crystals (70% yield), mp. 193.2 °C. Calculated for $C_{25}H_{29}Cl_2N_5O_{12}S$: C, 39.87; H, 3.88; N, 9.30. Found: C; 39.87; H, 3.81; N, 9.06%; ES-MS: m/z 570. λ_{max} (nm) (CH_3CN) 229 (ε ($dm^3\ mol^{-1}\ cm^{-1}$) 3481) 263 (2476.4). ν (cm^{-1}) (KBr discs) 3422b (O–H) (S–N), 1609m, 1586, 1449m (C=C) (C=N), 1329m (S=O), 1090s (ClO_4^-).

L · Co(II): procedure as described above, using $[Co(H_2O)_6]ClO_4$ (1.21×10^{-4} mol) except solution was placed in a butyl ether atmosphere. Complex was collected as pink crystals (55% yield), mp. 182.4 °C. Calculated for $C_{27}H_{34}Cl_2N_6O_{13}SCo$: C, 39.91; H, 4.22; N, 10.34. Found: C; 38.91; H, 3.88; N, 10.12%; ESMS: m/z 472.49. λ_{max} (nm) (CH_3CN) 223.5 (ε ($dm^3\ mol^{-1}\ cm^{-1}$) 6509) 272.5 (1884.4). ν (cm^{-1}) (KBr discs) 3386b (O–H) (S–N), 1610m, 1580, 1440m (C=C) (C=N), 1353m (S=O), 1089s (ClO_4^-).

L · Fe(II): procedure as described above, using $[Fe(H_2O)_6]ClO_4$ (1.21×10^{-4} mol). Complex was collected as brown crystals (73% yield), mp. 190.7 °C. Calculated for $C_{25}H_{29}Cl_2N_5O_{12}SCFe$: C, 40.02; H, 3.90; N, 9.33. Found: C; 39.95; H, 3.65; N, 9.04%; ES-MS: m/z 466.43. λ_{max} (nm) (CH_3CN) 267.3 (ε ($dm^3\ mol^{-1}\ cm^{-1}$)

2271) 230.8 (6084). ν (cm^{-1}) (KBr discs) 3421b (O–H), 2923m (S–N), 1610m, 1581m, 1447m (C=C), 1345m (S=O), 1161s, 1098s (ClO_4^-).

6. Supplementary material

Additional crystallographic material is available from the Cambridge Crystallographic Data Centre comprises relevant tables of atomic coordinations, bond lengths and angles and thermal parameters (CCDC = **L** [187242]; **L · Fe(II)** [185418]; **L · Co(II)** [185419]; **L · Ni(II)** [185420]; **L · Zn(II)** [187241]; **L · Co(II)** [185421]). Copies of this data may be obtained free of charge on application to The Director, CCDC, 12 Union Road, Cambridge CB2 1EZ, UK (fax: +44-1223-336033; e-mail: deposit@cam.ac.uk or www:http://www.ccdc.cam.ac.uk).

Acknowledgements

This work was supported by the HEA (Higher Education Authority) under the PRTLI 98 (Molecular Cell Biology Programme) research scheme, the Department of Chemistry Trinity College Dublin (Krieble Fund 2001–2002) and Kinerton Ltd. We thank Professor D. Clive Williams (Biochemistry, TCD) for his continuous encouragement and support, and Dr. Hazel M. Moncrieff, Dr. Paul E. Kruger and Dr. Emma R. Schofield for valuable discussions, and Dr. John E. O'Brien for assisting in the running of NMR.

References

[1] (a) B. Armitage, Chem. Rev. 98 (1989) 1171;
(b) K.E. Erkkila, D.T. Odom, J.K. Barton, Chem. Rev. 99 (1999) 2777;
(c) E.C. Long, Acc. Chem. Res. 32 (1999) 827.
[2] (a) E. Kimura, Acc. Chem. Res. 34 (2001) 171;
(b) N.V. Kaminskaia, B. Spingle, S.J. Lippard, J. Am. Chem. Soc. 123 (2001) 6555;
(c) N.V. Kaminskaia, C. He, S.J. Lippard, Inorg. Chem. 93 (2000) 3365;
(d) A.J. Kirby, Angew. Chem., Int. Ed. Engl. 35 (1996) 707;
(e) E. Kimura, Prog. Inorg. Chem. 41 (1994) 443;
(f) A.J. Kirby, Angew. Chem., Int. Ed. Engl. 33 (1994) 551.
[3] D.E. Wilcox, Chem. Rev. 96 (1996) 2435.
[4] (a) N.H. Williams, B. Takasaki, J. Chin, Acc. Chem. Res. 32 (1999) 485;
(b) D.S. Sigman, A. Mazumder, D.M. Perrin, Chem. Rev. 93 (1993) 2295;
(c) J. Chin, Acc. Chem. Res. 24 (1991) 145.
[5] (a) D.M. Perreault, E.V. Anslyn, Angew. Chem., Int. Ed. Engl. 36 (1997) 432;
(b) N. Sträter, W.N. Lipcomb, T. Klablunde, B. Krebs, Angew. Chem., Int. Ed. Engl. 35 (1996) 2024.
[6] (a) R. Häner, Chemia 55 (2001) 286;
(b) C.J. Leumann, Chemia 55 (2001) 295;
(c) W.S. Santora, G.F. Joyce, Proc. Natl. Acad. Sci. USA 94 (1997) 4262.
[7] (a) P. Gómez-Tagle, A.K. Yatsimirsky, Inorg. Chem. 40 (2001) 3786;
(b) T.A. Osiek, J.K. Baskin, New J. Chem. 25 (2001) 541;
(c) U. Baykal, M.S. Akkaya, E.U. Akkaya, J. Mol. Cat. A. 145 (1999) 309;
(d) A. Kuzuya, M. Akai, M. Komiyama, Chem. Lett. (1999) 1035;
(e) U. Baykal, E.U. Akkaya, Tetrahedron Lett. 39 (1998) 5861;
(f) M. Kalesse, A. Loos, Bioorg. Med. Chem. Lett. (1996) 2063;
(g) K.G. Ragunathan, H.-J. Schneider, Angew. Chem., Int. Ed. Engl. 35 (1996) 1219;
(h) P. Hurst, B.K. Takasaki, J. Chin, J. Am. Chem. Soc. 118 (1996) 9982;
(i) M. Yashiro, A. Ishikubo, T. Takarada, M. Komiyama, Chem. Lett. (1995) 655;
(j) K.O.A. Chin, J.R. Morrow, Inorg. Chem. 33 (1994) 5036;
(k) N. Hayashi, N. Takeda, T. Shiiba, M. Yashiro, K. Watanabe, M. Komiyama, Inorg. Chem. 32 (1993) 5899;
(l) H.-J. Schneider, J. Rammo, R. Hettich, Angew. Chem., Int. Ed. Engl. 32 (1993) 1716;
(m) J.R. Morrow, L.A. Buttrey, V.M. Shelton, K.A. Berack, J. Am. Chem. Soc. 114 (1992) 1903.
[8] (a) P. Molenveld, J.F.J. Engbersen, D.M. Reinhoudt, Chem. Soc. Rev. 29 (2000) 75;
(b) A. Roigh, H.-J. Schneider, Eur. J. Org. Chem. (2001) 205;
(c) P. Molenveld, J.F.J. Engbersen, D.M. Reinhoudt, Angew. Chem., Int. Ed. Engl. 38 (1999) 3189;
(d) P. Molenveld, J.F.J. Engbersen, D.M. Reinhoudt, J. Am. Chem. Soc. 119 (1997) 2948;
(e) S. Liu, Z. Lou, A.D. Hamilton, Angew. Chem., Int. Ed. Engl. 36 (1997) 2678;
(f) W.H. Chapman Jr., R. Breslow, J. Am. Chem. Soc. 117 (1995) 5462;
(g) M. Wall, R.C. Hynes, J. Chin, Angew. Chem., Int. Ed. Engl. 32 (1993) 1633;
(h) Chung, E.U. Akkaya, T.K. Venkatachalam, A.W. Czarnik, Tetrahedron Lett. 38 (1990) 5413.
[9] (a) B.N. Trawick, A.T. Daniher, J.K. Bashkin, Chem. Rev. 98 (1998) 939;
(b) R. Häner, J. Hall, A. Pfützer, D. Hüsker, Pure Appl. Chem. 70 (1998) 111;
(c) D. Magda, M. Wright, S. Crofts, A. Lin, J.L. Sessler, J. Am. Chem. Soc. 119 (1997) 6947;
(d) J. Hall, D. Hüsker, R. Häner, Nucleic Acid Res. 24 (1996) 3522.
[10] W.C. Putnam, A.T. Daniher, B.N. Trwick, J.K. Bashkin, Nucleic Acid Res. 29 (2001) 2199.
[11] (a) T. Gunnlaugsson, R.J.H. Davies, M. Nieuwenhuyzen, C.S. Stevenson, J.E. O'Brein, S. Mulready, Polyhedron 22 (2003) 711;
(b) T. Gunnlaugsson, R.J.H. Davies, M. Nieuwenhuyzen, C.S. Stevenson, R. Viguier, S. Mulready, Chem. Commun. (2002) 2136;
(c) T. Gunnlaugsson, J.E. O'Brein, S. Mulready, Tetrahedron Lett. 43 (2002) 8493.
[12] (a) T. Gunnlaugsson, A.J. Harte, J.P. Leonard, M. Nieuwenhuyzen, Chem. Commun. (2002) 2134;
(b) T. Gunnlaugsson, D.A. Mac Dónaill, D. Parker, J. Am. Chem. Soc. 123 (2001) 12866;
(c) T. Gunnlaugsson, Tetrahedron Lett. 42 (2001) 8901;
(d) T. Gunnlaugsson, D.A. Mac Dónaill, D. Parker, Chem. Commun. (2000) 93.
[13] G. Lee, M. Oka, M. Takemura, Y. Miyahara, N. Shimizu, T. Inazu, J. Org. Chem. 61 (1996) 804.
[14] R. Breslow, D.-L. Huang, Proc. Natl. Acad. Sci. USA 88 (1991) 4080.
[15] SAINT-NT, Brüker AXS Madison, Wisconsin, 1998.

[16] G.M. Sheldrick, University of Göttingen, Göttingen, Germany, 1998.
[17] (a) T. Gunnlaugsson, M. Nieuwenhuyzen, L. Richard, V. Thoss, J. Chem. Soc., Perkin Trans. 2 (2002) 141;
(b) T. Gunnalugsson, A.P. Davis, J.E. O'Brien, M. Glynn, Org. Lett. 4 (2002) 2449;
(c) T. Gunnlaugsson, A.P. Davis, M. Glynn, Chem. Commun. (2001) 2556.
[18] S. Aime, A.S. Batsanov, M. Botta, R.S,. Dickins, S. Faulkner, C.E. Foster, A. Harrison, J.A.K. Howard, J.M. Moloney, T.J. Norman, D. Parker, L. Royle, J.A.G. Williams, J. Chem. Soc., Dalton Trans. (1995) 2259.